Polymer Journal, Vol. 39, No. 12, pp. 1221–1237 (2007)


SPECIAL ISSUES -PROGRESS IN STRUCTURE ANALYSES OF POLYMERIC MATERIALS BY SYNCHROTRON RADIATION AND NEUTRON BEAM- REVIEW ARTICLE

# Application of Microbeam Small- and Wide-angle X-ray Scattering to Polymeric Material Characterization

Yoshinobu NOZUE,[1,†] Yuya SHINOHARA,[2] and Yoshiyuki AMEMIYA[2]

[1]*Sumitomo Chemical Co., Ltd., Petrochemicals Research Laboratory, Kitasode, Japan*
[2]*Department of Advanced Materials Science, Graduate School of Frontier Sciences, The University of Tokyo, Kashiwa, Japan*

(Received June 15, 2007; Accepted September 26, 2007; Published October 31, 2007)

ABSTRACT: With the recent development of an X-ray source, focusing optics, and X-ray detectors, microbeam X-ray scattering techniques have been well established and widely applied to the characterization of polymeric materials. Microbeam X-ray scattering is a unique and powerful tool that provides abundant information on local structures, such as the spatial inhomogeneity of materials and the structural change at a local position. Furthermore, by combining microbeam small-angle X-ray scattering (SAXS) and wide-angle X-ray scattering (WAXS), the observable spatial scale range is from several to several hundred Å, which is the most important scale range in the hierarchical structure analyses of polymers. In this review, the representative applications of microbeam X-ray scattering to polymer crystallization, spatial inhomogeneity analyses, stress transfer under external field and the microphase separated structure analyses in block copolymer systems are introduced. [doi:10.1295/polymj.PJ2007077]

KEY WORDS Microbeam Small- and Wide-angle X-ray Scattering / Polymer Characterization /

X-Ray scattering techniques are widely applied to the observation of various polymer structures. X-Ray scattering is mainly classified into small-angle X-ray scattering (SAXS) and wide-angle X-ray scattering (WAXS), depending on the scattering angle. As is easily understood by using the Bragg formula ($\lambda = 2d \sin\theta$), when the scattering angle $2\theta$ decreases, scattering reflects a large structure. SAXS, which is X-ray scattering at small angle ($< 2, 3^\circ$) region, provides information on nanostructures in a size range of several to several ten nanometers. In the field of polymeric materials, SAXS is typically applied to obtaining information on crystalline lamella stacking structures,[1,2] various microphase separated structures in block copolymer systems,[3,4] and organic-inorganic composite structures.[5,6] On the other hand, WAXS is typically applied to obtaining information on sub-nanometer-scale structures, such as crystal packing and amorphous structures.

To determine the structural characteristics of polymeric materials in detail, it is also very important to understand the formation and/or deformation mechanisms of such materials. Although X-ray scattering experiments were limited to the static measurements in laboratory X-ray sources until early 1980s, the advent of a synchrotron X-ray source and the development of X-ray detectors[7–13] have enabled us to observe a one- or two-dimensional scattering pattern within a second, making it possible to perform time-resolved X-ray scattering measurements for various structural changes, such as crystallization,[14–17] structural changes due to deformation[18–23] and phase transition due to temperature change.[24–26] While many polymeric materials exhibit spatial inhomogeneity on a micrometer scale, conventional X-ray scattering techniques provide the information that is spatially averaged over more than hundreds micrometer of the sample area irradiated by X-ray beam. Structural inmhomogeneity sometimes plays a very important role in controlling mechanical and optical properties. Even a conventional time-resolved X-ray scattering measurement technique is not sufficient for understanding such cases. Therefore, a microbeam X-ray scattering technique is necessary for obtaining the local structural information and structural inhomogeneity.

Historically, the first microbeam X-ray scattering application to a polymer for the analysis of banding spherulite was reported in 1955 by Keller.[27] At that time, a microbeam of 8 μm diameter was obtained from a laboratory X-ray source using a collimator, and the exposure time for data acquisition was several hours. Since then, X-ray focusing optics, which are described in the following section, and synchrotron X-ray radiation sources with a high brilliance (high parallelism and high flux) have been continuously developed. With these new apparatuses, we can obtain an X-ray microbeam with a high parallelism and a high flux, which is suitable for observing a scattering

[†]To whom correspondence should be addressed (Tel: +81-436-61-1120, E-mail: nozue@sc.sumitomo-chem.co.jp).

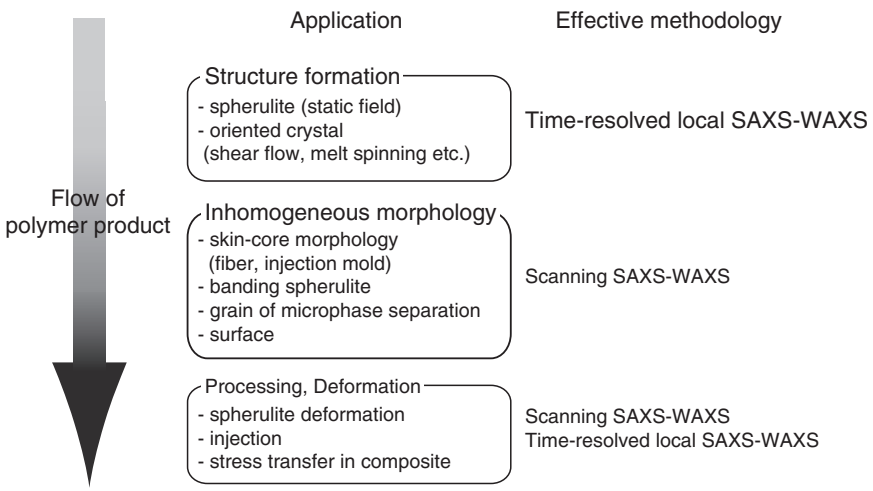


**Figure 1.** Application of microbeam XRD to polymer characterization.

pattern in a μm-scale local region within several seconds. Currently, there exist several beamlines for microbeam X-ray scattering experiments in ESRF,[28,29] APS,[30] SPring-8,[31] BESSY II,[32,33] and PF.[34,35]

Microbeam X-ray scattering techniques are classified into a time-resolved local X-ray scattering method and a scanning X-ray scattering method. The former is the method for observing the time variation of a local structure by pinpointing a fixed area with a microbeam X-ray. The latter is the method for observing scattering patterns at various areas by scanning a sample with an X-ray microbeam. Typical applications of these techniques to polymer science are summarized in Figure 1.

In this review, we first introduce the X-ray optics for microbeam generation and then the recent representative applications of microbeam X-ray scattering to polymeric material characterization. In the application section, we introduce the crystallization (in 3.1), inhomogeneous crystalline morphology (in 3.2), and deformation of a crystalline polymer (in 3.3), the order of which is analogous to a life cycle of polymeric materials. In addition, we introduce the rare application of microbeam X-ray scattering to a microphase separated noncrystalline block copolymer system in 3.4.

## X-RAY OPTICS FOR GENERATING MICROBEAM X-RAY

To perform microbeam X-ray diffraction/scattering experiments, especially microbeam SAXS, a highly collimated microsized X-ray beam with a high flux is required. Because the product of spatial and angular divergences is kept in a constant flux (Liuville's theorem), we cannot obtain a microbeam from a macrobeam without changing the angular divergence and its intensity. Therefore, a synchrotron X-ray radiation source with an extremely high brilliance and efficient focusing optics are required.

There exist various optical systems for generating an X-ray microbeam (As for the review of focusing optics, see ref 36). Typical optical systems are shown in Figure 2. They are mainly classified into focusing and pinhole optics. As for the focusing optics, the following optical instruments are often used: (a) glass capillary, which selects the beam with a divergence angle smaller than the critical angle of inner glass surface, (b) a Kirkpatrick-Baez (K-B) focusing mirror system,[37] which consists of two bent mirrors independently focusing in the horizontal and vertical directions, (c) a refractive lens,[38] which is based on the fact that the reflactive index of a material for X-rays is less than 1, (d) an X-ray zone plate,[39] which selects X-rays with phases that interfere with each other by concentrically shaped patterning, (e) a Bragg-Fresnel lens,[40] which utilizes the confocal property of ellipsoid, (f) an X-ray waveguide,[41] which generates standing wave. A glass capillary has a good property in that the shape of X-ray beam is almost kept constant through microbeam generation. A K-B focusing mirror, a refractive lens, an X-ray zone plate, a Bragg-Fresnel lens, and an X-ray waveguide are the state-of-art focusing optics, each of which has an ability to generate a submicrobeam or a nanobeam when it is used with an X-ray source of high brilliance such as a third generation synchrotron source. Most instruments are used in combination with a downstream small aperture, which blocks the parasitic scattering from upstream focusing optical systems.

As for the pinhole optical system, a microbeam is generated using micropinholes with diameters of several micrometers. Microbeam experiments using a micropinhole system require the preparation of pinholes with very clear edges and, more critically, the use of an X-ray source with an extremely high brilli-

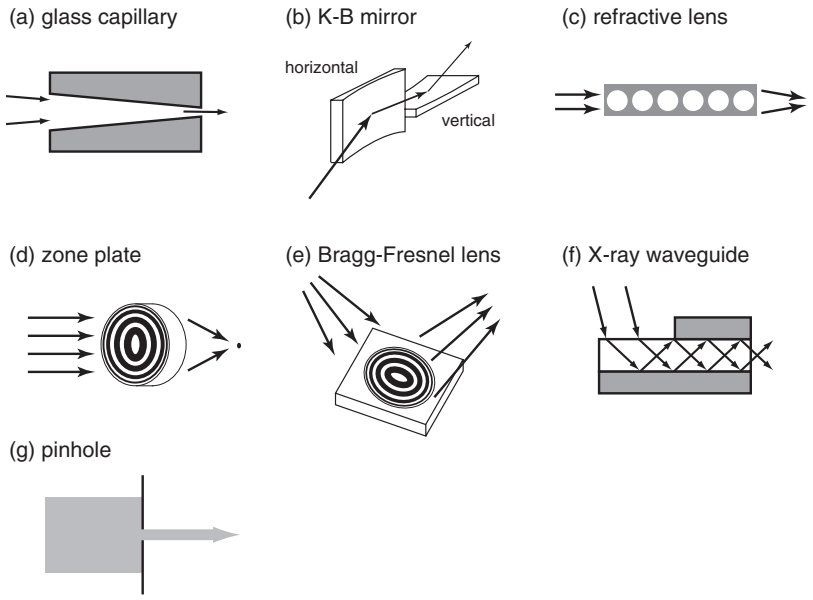


**Figure 2.** Schematic views of X-ray optics for X-ray microbeam generation.

ance, such as a pink beam beamline without a monochromator.[42] Furthermore, it should be noted that the size of the microbeam generated with a micropinhole is increased by Fraunhofer diffraction when the distance from the micropinhole increases.

There are several methods available to determine the beam position of a generated micobeam. One of the examples is a method to use crossed thin wires. The position of a microbeam is identified by moving a thin metal wire with several μm diameter across the X-ray microbeam while monitoring the transmitted X-ray intensity with an ionization chamber: the transmitted intensity becomes minimum when the positions of microbeam and the crossed wires completely coincide with each other, In the method with cross wire, one can also monitor the scattering pattern with SAXS detector instead of transmission. If a microbeam hits a wire, strong streak pattern appears due to the reflection at the surface of the wire. In this case, the position where the strong crossed streak scattering pattern appears will be equivalent with that where the transmitted intensity is minimized. Another method to locate the position of a microbeam is to use X-ray sensitive paper, the color of which is changed as a response to X-ray with a high spatial resolution.

## APPLICATIONS OF MICROBEAM SMALL- AND WIDE-ANGLE X-RAY SCATTERING

### *Crystallization Process*

Polymer spherulites, such as banding,[27,43,44] interpenetrating,[45,46] and cross-hatched spherulites,[47] have complex structures. Even in a simple polymer spherulite, primary and secondary crystallized lamellae coexist within a single spherulite.[48,49] For understanding the formation mechanism of such complex morphologies, the observation of the crystallization behavior at a growth front of a spherulite is a very effective method.[50–52] In addition to crystallization in static fields, polymer crystallization during processes, such as injection,[53] inflation[54] and spinning,[55] is also very important and widely studied because such external force fields strongly affect the formation of crystalline morphologies such as a shish-kebab structure.[56,57] Furthermore, when the processed materials themselves are very small[58] or spatially heterogeneous,[59] the structural information obtained during crystallization at a local position is essential for understanding their formation mechanism in detail.

In such systems, a microbeam X-ray scattering method is suitable for observing crystallization processes at a local position.[50–52,58,59] In this section, three applications of a microbeam to polymer crystallization are introduced. The first two applications are related to spherulite growth and the third application to the crystallization of the strongest natural fiber, spider silk.

*Growth of Spherulite.* A polymer blend system that has two kinds of lamella within a spherulite, poly($\varepsilon$-caprolactone) (PCL)/polyvinylbutyral (PVB), is known as a blend system that forms a very large banding spherulite with a high twisting order.[60] PVB molecules, which can interact with PCL through hydrogen bonding, strongly disturb the crystallization of PCL and the crystal nucleation frequency is depressed by two orders of magnitude.[60] The other interesting characteristic is the coexistence of two types of lamella having different long periods within a spherulite. The information on the formation sequence of two lamellae allows us to interpret the origin of the two kinds of lamella. An X-ray microbeam of $4 \times 5\,\mu m^2$,

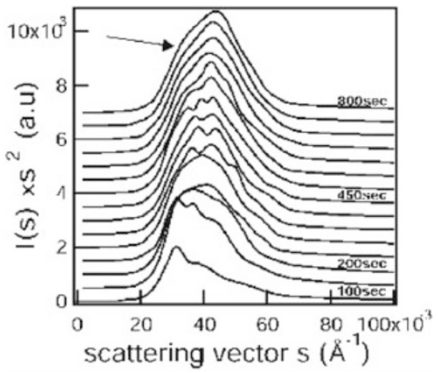


**Figure 3.** SAXS profiles of PCL/PVB during crystallization with X-ray microbeam positioned immediately outside growth front of the band spherulite. See the text about the arrow. (Reprinted with permission from ref 51. Copyright (2003) Elsevier Ltd.).

which was generated with K-B mirror optics, was initially fixed at the outside vicinity of the growth front of spherulites. As the spherulite grew, the growth front of spherulite crossed the microbeam, and the time evolution of local crystallization was observed with two-dimensional SAXS.[51] A change in SAXS profiles during crystallization at the fixed position is shown in Figure 3. The growth rate was determined to be 8.1 μm/min with a polarized optical microscope. The interval of data acquisition and the exposure time was 50 s and 16 s, respectively. At $t = 100$ s, scattering from the crystal started to be observed, which suggests that the growth front of spherulite crossed the X-ray microbeam at $50\,\text{s} < t < 100\,\text{s}$. From Figure 3, we can clearly observe the primary formation of lamellae with a larger long period, followed by the formation of lamellae with a shorter long period, which is similar to that of PCL lamellae without PVB. As previously reported,[60] the shoulder at a smaller scattering vector (see the arrow in Figure 3) in the scattering profile clearly remains until the end of crystallization, showing that both the larger and shorter components of lamellae coexist at the end of crystallization. From this result, the authors suggested that the primary formation of lamellae with a larger long period is strongly affected by the existence of PVB molecules, which is eventually excluded from PCL crystallites. The strong interaction between PCL and PVB influences the formation of larger lamellae long period.

The second application is the observation of interpenetrating spherulite formation. The growth of polymer spherulite typically stops by impingement between neighboring spherulites. Recently, interpenetration in a miscible crystalline/crystalline polymer blend system, where the lamella of 'polymer A' penetrates the as-formed spherulite of 'polymer B',[45,46] has been discovered. However, its degree of penetration (interfibril or interlamella region) had not yet been clarified. Nozue *et al.* investigated an interpenetrating behavior in a poly(butylene succinate) (PBSU)/poly(vinyl chloride-co-vinylidene chloride) (P(VDC-VC)) blend by simultaneous microbeam SAXS-WAXS measurement.[52] They pinpointed P(VDC-VC) spherulite, which was formed earlier, with an X-ray microbeam ($\lambda = 1.0$ Å, the beam size $\sim 10$ μm diameter) generated with pinhole optics and observed the penetration process of subsequently growing PBSU spherulite into P(VDC-VC). A change in a polarized optical microscopy (POM) image during interpenetration is shown in Figure 4 and the corresponding SAXS-WAXS patterns are shown in Figure 5. The white filled circle in Figure 4 shows the position where the X-ray microbeam was irradiated. From Figure 5, one can clearly observe a drastic change in central scattering intensity ($s < 0.04\,\text{Å}^{-1}$), which mainly originates from the fibril structure of P(VDC-VC). Initially, central scattering largely increases and then decreases when the weak peak of the long period at around $0.045\,\text{Å}^{-1}$ and the WAXS peak of the PBSU crystal appear. This fact indicates that the penetration of PBSU with stacked lamellae occurred in the interfibril region.

*Crystallization of Spider Silk Fiber.* It is well known that spider silk fiber is one of the strongest fibers found in nature and its formation mechanism is very interesting because it is the best model for a strong fiber design. However, spider silk fiber has a diameter of several micrometers and it is necessary to perform microbeam X-ray diffraction measurement for the direct observation of the crystallization behavior. Riekel *et al.* performed very unique *in situ* measurements of spider silk crystallization.[58,61,62] They fixed the *Nephila senigalensis* spider using soft tape and mylar bandages to a metal support and forced it to silk by reeling the fiber with a spindle (see Figure 6). They irradiated the spinning path at various positions with a microbeam of 10 μm diameter, which is generated with glass capillary optics, and observed structure evolution during spinning.[58] At 2.4 mm from the spinneret, oriented amorphous and crystal structures were observed, though their crystallinity was very low. Interestingly, diffraction data acquired at distances $\geq 2.4$ mm from the spinneret showed that the orientation degrees of the crystal structures remain constant, while their crystallinity simply increases. Furthermore, their observed changes in the degree of orientation under various spindle drawing speeds showed a higher degree of orientation than those observed by Kevler when drawing speed is faster than 25 mm/s. They concluded that *not* post-extrusion draw down *but* the speed of drawing constrains the molecular order, thus affecting the mechanical properties of fibers.

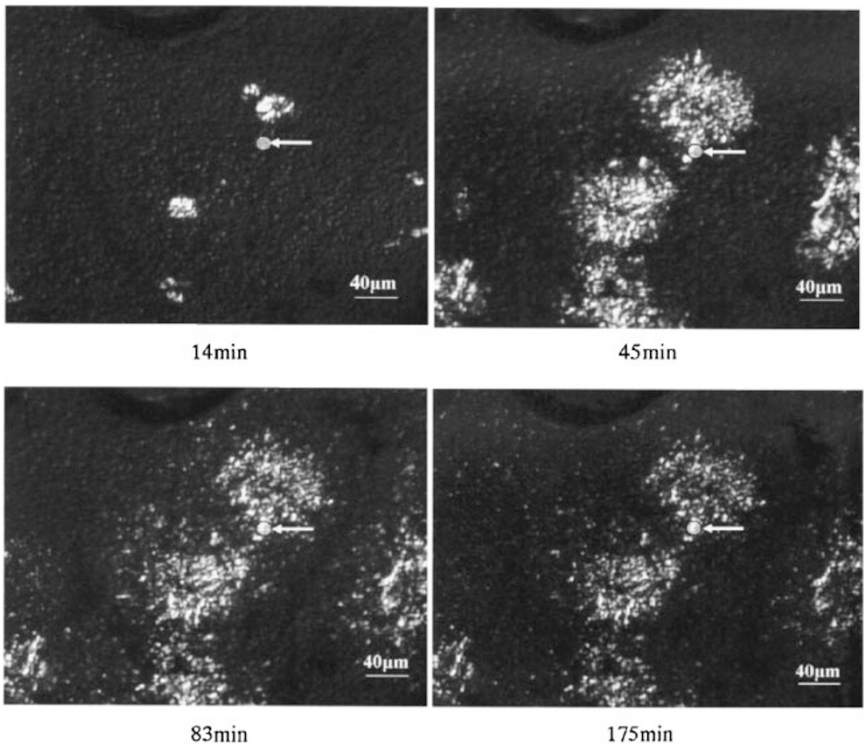


**Figure 4.** Change in microscope image of PBSU/P(VDC-VC) = 60/40 during isothermal crystallization at 95 °C. The circle indicated by the arrow in each image shows the position of the X-ray microbeam (Reprinted with permission from ref 52. Copyright (2004) Elsevier Ltd.).

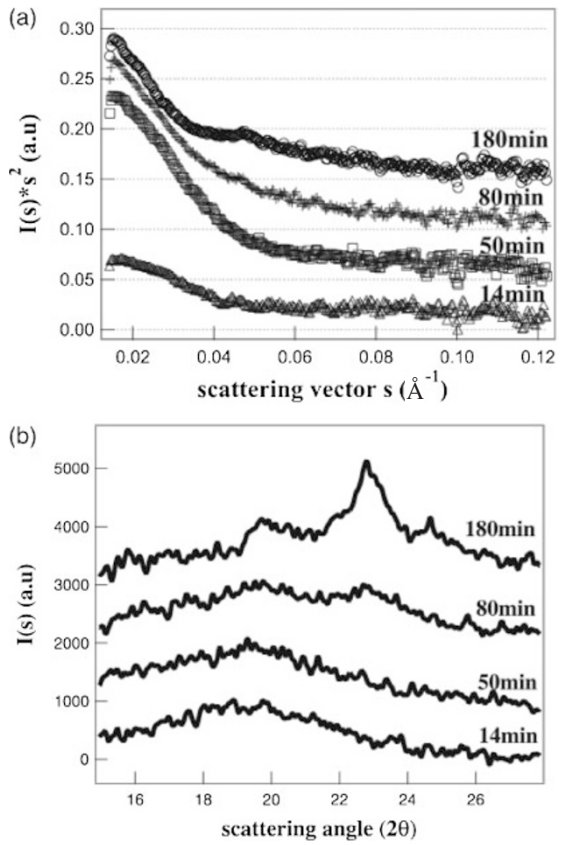


**Figure 5.** Time development of microbeam SAXS (A) and WAXS (B) during interpenetration (Reprinted with permission from ref 52. Copyright (2004) Elsevier Ltd.). SAXS and WAXS profiles are vertically shifted for clarity.

*Inhomogeneous Crystalline Morphology*

Polymer crystalline morphologies exhibit spatial inhomogeneity on a micrometer scale, which are strongly affected by various factors controlling crystallization. In this section, we show microbeam X-ray scattering applications to three representative crystalline morphologies with spatial inhomogeneity: banding spherulite, a cylindritic structure and a lateral structure in a fiber.

*Twisting Lamella Structure in Banding Spherulite.* Banding spherulite has a concentric ring morphology, as observed under POM which is formed by the twisting of crystalline lamellae with birefringence. It has been investigated over the past 40 years and its detailed twisting mechanism has been the center of debates until now. As is described in Introduction, the first microbeam WAXS experiment was applied to the banding spherulite of polyethylene in 1955.[27] Recently, it has been understood that the origin of lamella twisting varies from polymer to polymer. For example, in polymers with a growth front tilting toward the growth direction, lamella twisting seems to be due to the torque produced by the density difference on the growth front of lamellae owing to the tilting of the c-axis.[44,63] In the case of polymers with chiral structures, it is considered that the chirality of the main chain is the origin of lamella twisting and that it is strongly related to the handedness of lamella twisting.[64,65] Furthermore, lamella twisting has also been

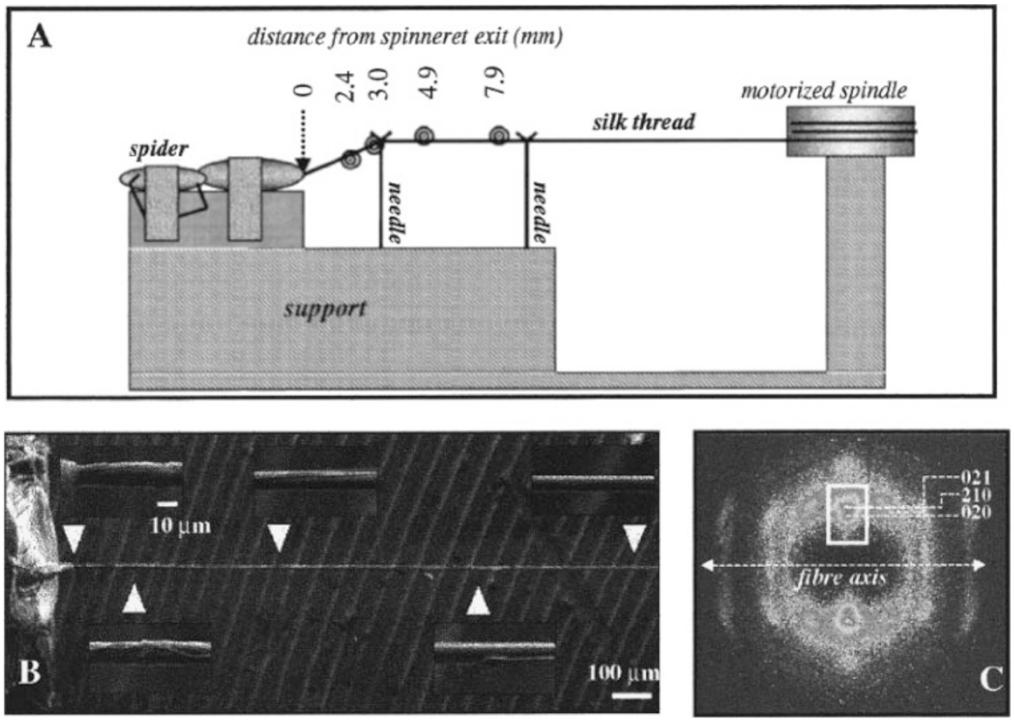


**Figure 6.** (A) Experimental setup for *in situ* X-ray diffraction during forced silking. The spider is fixed using soft tape and Mylar bandages to a metal support. The path of the thread from the spinneret to the motorized reel is schematically indicated. Distance indications (to the spigot exit) correspond to points where X-ray diffraction data were recorded. (B) SEM image of draw down of *N. edulis* spider silk at drawing speed of 20 mm/s. (C) Diffraction pattern obtained at $23.5 \pm 0.5\,^{\circ}$C. Miller's indices indicated for selected reflections (Reprinted with permission from ref 58. Copyright (2000) American Chemical Society).

found in some crystalline/amorphous polymer blend systems that have neither chirality nor c-axis tilting in a crystal. In this section, we focus on the twisting manner in crystalline/amorphous polymer blend system.

Nozue *et al.* performed microbeam scanning SAXS/WAXS measurements for the detailed structural analysis of banding spherulite in a PCL/PVB blend.[51,66] This blend is one of the most ideal systems because the order of twisting is extraordinarily high and the period of twisting is sufficiently large to perform a microbeam scanning experiment. They scanned isothermally crystallized banding spherulite along the radial direction with a microbeam generated with K-B optics (the beam size was $4 \times 5\,\mu m^2$) and observed the difference between banding structures formed at different isothermal crystallization temperatures.[51] They calculated the azimuthal distribution of 110 reflection intensity in each scanned image. On the left side of Figure 7, a variation in the azimuthal distribution of the 110 reflection during scanning is shown, and a clear difference in twisting manner is observed between banding spherulites isothermally crystallized at 35 and 41 °C. To interpret the difference in azimuthal distribution change, they calculated the azimuthal distribution change in various twisting manners by assuming that the reciprocal lattice point corresponding to the 110 reflection has a Gaussian distribution. The calculated results are shown on the right side of Figure 7 together with the twisting modes used for calculation. By comparing the experimental and calculated azimuthal distributions, one can clearly observe that the banding spherulite crystallized at 37 °C twists uniformly, whereas that crystallized at 41 °C twists in a stepwise manner. They considered that stepwise twisting is strongly related to the rhythmic growth of the previously reported banding spherulite.[67] Furthermore, another interesting characteristic was found in this banding spherulite. It is known that some banding spherulites including PCL/PVB have radial lines from the center of the spherulite. To clarify the origin of these radial lines, the banding structures on the left and right sides of the radial lines were scanned with a microbeam and the periodic changes in the azimuthal distribution of the 110 reflection were compared[66] (see Figure 8). The obtained results clearly show the inverse relationship of periodic patterns, indicating the inverse relationship of twisting handednesses. Thus, it is considered that a radial line indicates the boundary between different handednesses. In addition to PCL/PVB, Gazzano *et al.* investigated the twisting of poly(L-lactic acid) (PLLA) and its blend with atactic poly(3-hydroxybutyrate) (aPHB) by microbeam WAXS.[68] They also focused on the in-

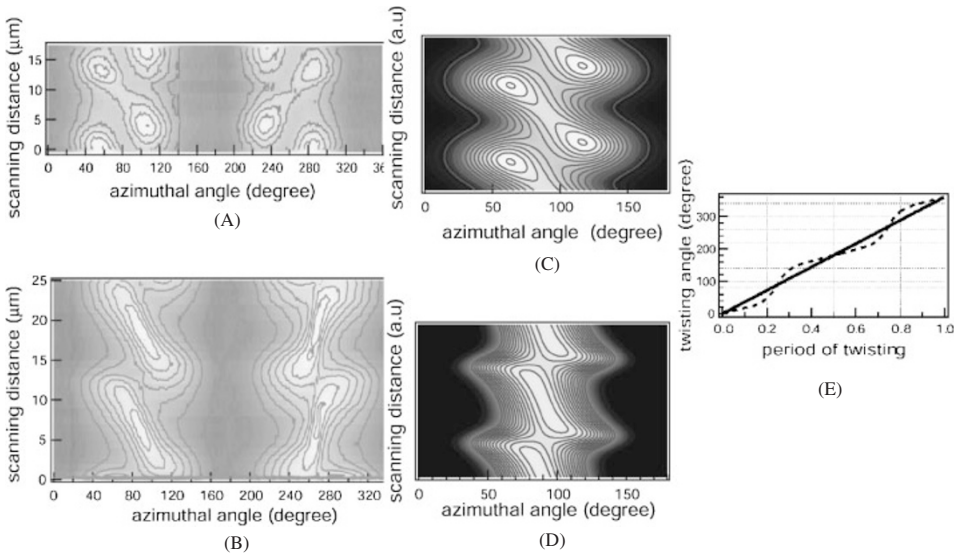


**Figure 7.** (left) WAXS intensity contour maps with X-ray microbeam scanning PCL/PVB spherulite isothermally crystallized at 35 °C (A) and 41 °C (B). (center, C and D) Simulated intensity contour map of 110 reflection azimuthal distribution along the radial direction. (C) Continuous twisting model and (D) step-like twisting model shown in (E). Definition of the azimuthal angle is shown in Figure 8 (Reprinted with permission from ref 51. Copyright (2003) Elsevier Ltd.).

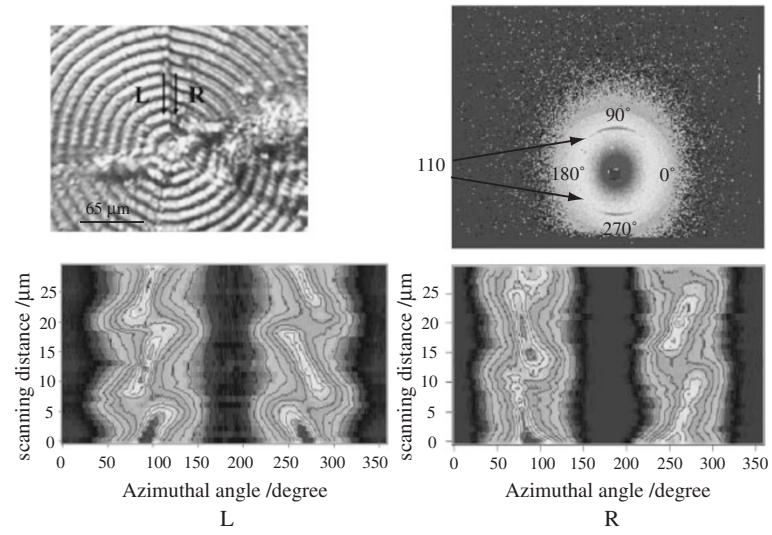


**Figure 8.** (upper left) POM image of PCL/PVB (95/5) crystallized at 41 °C. In this image, the 'line' in the radial direction is clearly observed. X-Ray microbeam scanning was performed along the line. (lower) Intensity contour maps of 110 reflection azimuthal distribution in WAXS with X-ray microbeam scanning L line (left) and R line (right) of PCL/PVB spherulite. The definition of azimuthal angle is shown in upper right figure, in which 110 reflection is indicated by arrows. (Reprinted with permission from ref 66. Copyright (2004) Elsevier Ltd.).

duction of twisting by adding an amorphous polymer. They excluded the possibility of any twisting with a large pitch in PLLA spherulite without blending aPHB and concluded that the twisting structure is purely induced by aPHB addition.

*Cylindritic Morphology of iPP β-Phase.* Recent tremendous research studies about polymer composites include fiber-reinforced polymeric materials. In such systems, not only the strength of a fiber but also the control of a matrix polymer morphology is very important for improving the reinforcement effect. In iPP, a $\beta$-phase crystal is known as a polymorph that improves mechanical properties.[69] It is also known that a $\beta$-phase is induced by the thermal gradient,[70] $\beta$-nucleating agent[71] and shear force.[72] As for the shear-induced oriented $\beta$-phase formation at the interface between iPP and the fiber, it was unclear whether the $\beta$-phase grows directly from the sheared interface (transcrystalline structure) or from an oriented $\alpha$-phase (cylindritic structure). To clarify the origin of $\beta$-phase formation, Torre *et al.* prepared an oriented $\beta$-phase morphology and performed a microbeam

WAXS experiment.[73] They sandwiched a fiber, Vectra A950 167TEX, which is a thermotropic main-chain liquid crystal polymer, between iPP films, heated it to 210 °C and held it for 5 min. Then, they decreased the temperature, pulled the fiber out at 140 °C and isothermally crystallized it at 135 °C. In Figure 9, the POM image of the oriented crystalline structure, which grows normal to the pull-out direction of Vectra, is shown. They scanned the sample with a microbeam (the beam size was 3 μm diameter) normal to the pull-out direction and obtained a WAXS pattern at each position as shown in the upper side of Figure 10. The contour map of the corresponding circularly averaged microbeam WAXS profiles is shown on the lower side of Figure 10. The result shown in Figure 10 indicates that iPP at the region nearest the sheared iPP/Vectra interface has a highly oriented $\alpha$-phase, while a $\beta$-phase grows from the oriented $\alpha$-phase, indicating a cylindritic structure.

*Fibrous Structure.* Microbeam X-ray scattering is most often applied to fiber structural analysis.[74–87] On

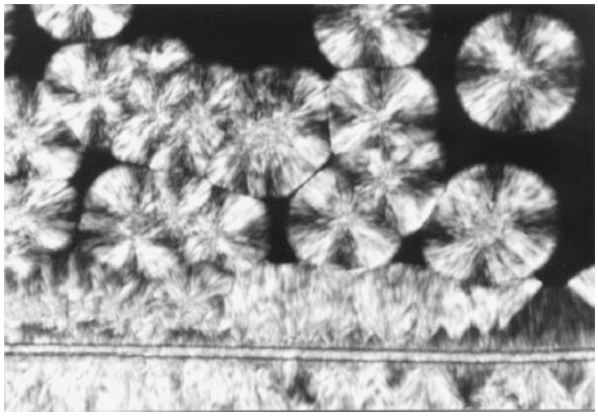

**Figure 9.** Crystalline superstructure formed by a Vectra A950 fiber (diameter: 23 μm) on an iPP matrix during isothermal crystallization at 135 °C. The fiber was previously pulled at 140 °C (Reprinted with permission from ref 73. Copyright (2006) American Chemical Society).

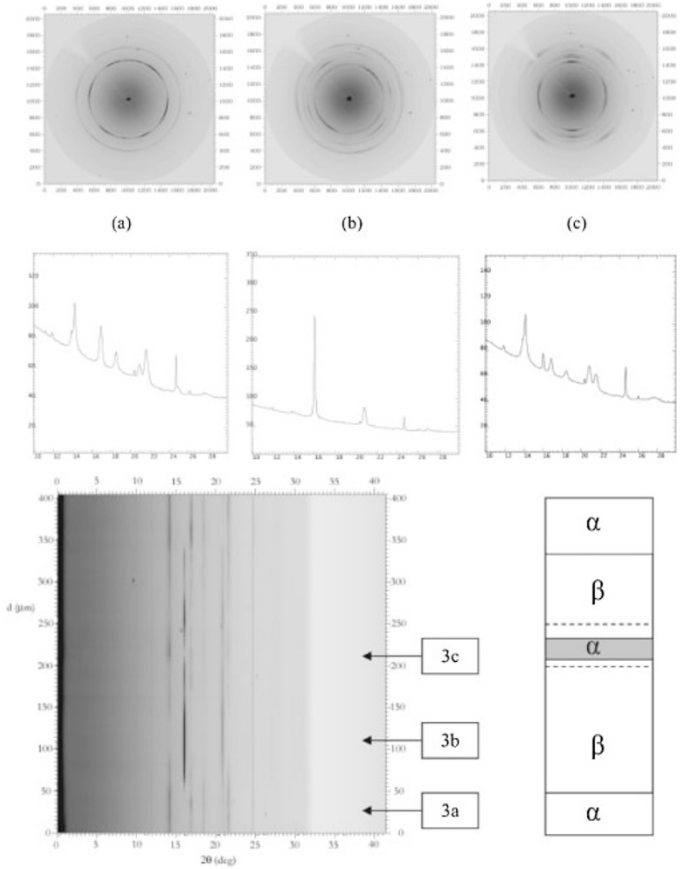


**Figure 10.** (upper) WAXS patterns of iPP matrix crystallized under isothermal conditions at 135 °C in which a Vectra fiber was pulled out at 140 °C. The sample was mapped from one side of the transcrystalline region to the other side with steps of 5 μm. (a) diffraction corresponding to spherulite of a-crystalline form, (b) pattern showing reflections for b-cylindritic structure and (c) WAXS pattern recorded at the region that the fiber occupied. (lower) Integrated intensities of X-ray diffraction patterns at different $2\theta$ angles for diffraction collected across sample covering large distance ($d$ μm) from one side of fiber to other side. The sample is an iPP matrix isothemally crystallized at 135 °C, in which a Vectra fiber was pulled out at 140 °C. The positions corresponding to the upper diffractograms are indicated as 3a, 3b, and 3c (Reprinted with permission from ref 73. Copyright (2006) American Chemical Society).

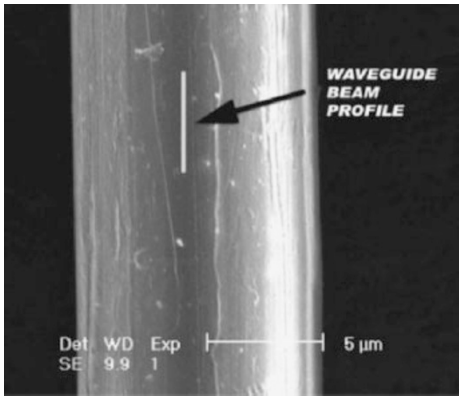


**Figure 11.** Schematic representation of waveguide beam profile superimposed to scale upon SEM micrograph of PBO HM fiber (Reprinted with permission from ref 84. Copyright (2005) American Chemical Society).

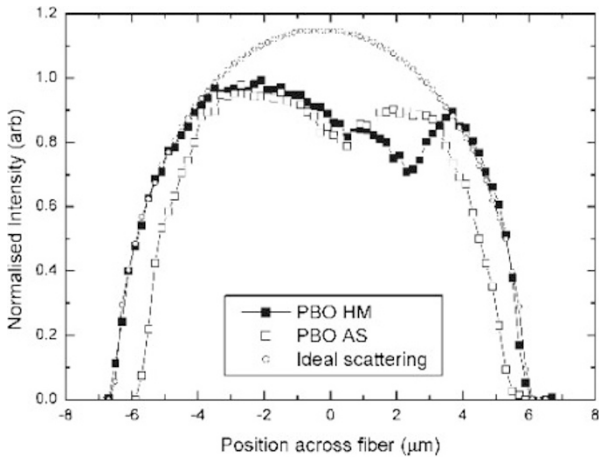


**Figure 12.** Across-fiber integrated intensity of 005 layer line of single PBO AS and HM fibers, and idealized scattering curve based on homogeneous cylindrical fiber (Reprinted with permission from ref 84. Copyright (2005) American Chemical Society).

the basis of simple suppositions, such as that on cylindrical symmetry, many researchers analyzed skin-core morphologies in a fiber. The most advanced application of X-ray microbeam to fiber analyses is a diffraction study using a sub-micrometer-sized X-ray beam.[84,85] An X-ray waveguide apparatus enables us to obtain highly focused X-ray 'submicrobeams' of 0.1 µm in one direction (see Figure 11). Davies *et al.* performed submicrobeam WAXS to obtain the detailed structural information of an inner structure in a poly(*p*-phenylenebenzobisoxazole) (PBO) fiber,[84] which is known as the superfiber with an extremely high strength and an extremely high elasticity. They scanned two samples, the as-spun PBO (PBO AS) and the high-modulus PBO (PBO HM) prepared by heat treatment, with submicrobeam across the fibers at 0.2 µm intervals and calculated the integrated intensity of a 005 layer line at each position,[84] which relates to crystallinity and orientation of crystals. From the patterns of integrated intensity across the fibers (see Figure 12), they simulated the detailed inner structure by Monte Carlo simulation based on three-phase model (skin, intermediate, and core region) with a simple supposition. They concluded that PBO AS has a thick outer skin layer with an amorphous structure and a symmetrical core region, which is located at the geometrical center of the fiber, whereas PBO HM has a very thin skin layer and a large disordered asymmetric core region, which is largely shifted from the geometrical center of the fiber. This large difference in inner structure between samples before and after heat treatment provides a clue to the structure-property relationship in fibers.

Next, we introduce the application of microbeam SAXS to the structural analysis of human hair.[86] Human hair shows various fiber shapes and it is commonly accepted that the degree of curliness of hair fibers are roughly classified on the basis of the ethnic origins of the hair fibers in three major ethnic groups: African hair is strongly curled, Caucasian hair is moderately wavy and Asian hair is comparatively straight. The origin of curliness attracts attention from the cosmetic viewpoint. It is widely known that the surface of human hair is covered with thin cells and its inner part is mainly filled with cortical cells, which are composed of the intermediate filaments surrounded by matrix proteins.[88] In the case of Merino wool, which is strongly curled, it was found that the fiber crimp is associated with the distribution of cortical cells, the so-called orthocortex and paracortex.[89] Kajiura *et al.* revealed the relationship between the curliness and inner structural morphology of human hair by microbeam SAXS.[86] They scanned single hair fibers with an X-ray microbeam generated with K-B mirror optics (the beam size was 6 µm diameter) and found that the arrangement of the intermediate filaments varies between the inner and outer sides of the curvature (Figure 13). They concluded that the macroscopic curliness of the hair fibers originates from the inhomogeneous distribution of two types of cortex from the analogy with Merino wool regardless of ethnic origin.

*Structural Change Due to Deformation*

To design polymeric materials with the required properties based on the structure-property relationship, it is essential to understand the pathway of stress transfer in deformation processes. Microbeam X-ray scattering is a powerful and unique tool for addressing issue because it can directly probe local structural deformation.[90–95] Furthermore, if one can perform *in situ* microbeam X-ray scattering measurement at a fixed position during deformation, further information on structural changes[90,92] will be obtained. However, it

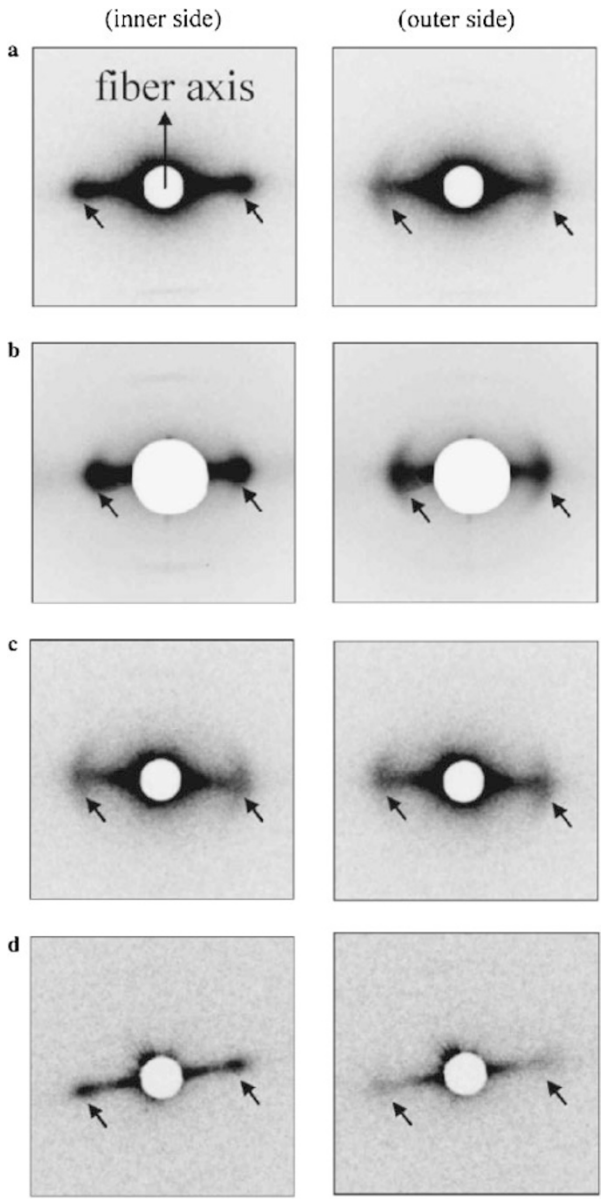


**Figure 13.** Typical SAXS patterns of human hairs for three ethnic groups and Merino wool ((Reprinted with permission from ref 86. Copyright (2006) Elsevier Ltd.)). (a) Curly African hair. (b) Moderately curly Caucasian hair. (c) Nearly straight Asian hair. (d) Merino wool with higher crimp than curly human hair. Short arrows indicate the major intensity maxima along the equator, which are attributed to the lateral packing between intermediate filaments (around 9.0 nm). Clear differences in these intensity maxima are found between the inner and the outer side of the curvature for the hairs. These differences reflect the existence of laterally heterogeneous intermediate filaments.

should be noted that well-designed sample accessories that apply a specific external force to a sample and monitor an exact X-ray beam position on the sample without interfering with the X-ray beam are necessary for *in situ* measurement. In this section, some advanced applications of microbeam X-ray scattering to the characterization of deformed materials are introduced.

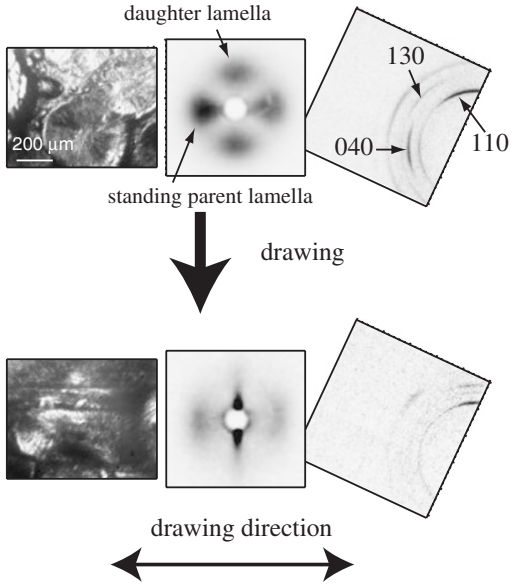


**Figure 14.** Typical data sets of POM (left), SAXS (center), and WAXS (right) before and after hot drawing. In the POM image, the position of the microbeam is shown by a dot (Reproduced with permission from ref 90. Copyright (2007) American Chemical Society).

*Elongation.* The first application is *in situ* microbeam SAXS-WAXS simultaneous measurement during the deformation of an iPP spherulite. iPP is one of the most widely used polyolefins for film applications. The most common process used for iPP film production is the tenter process, where an iPP sheet is stretched below its melting point by sequential biaxial drawing. Therefore, the understanding of the iPP spherulite deformation mechanism during drawing is very important for designing polypropylene materials with a high processability.

Nozue *et al.* observed microbeam SAXS-WAXS changes in an iPP spherulite at a fixed position during deformation using a drawing machine with a position-adjusting function independent of drawing. In Figure 14, the sets of POM-μSAXS-WAXS data simultaneously acquired before and after hot drawing are shown. They irradiated the dot region of POM image with a microbeam generated with pinhole optics (the beam size was 5 μm diameter) and obtained μSAXS-WAXS data. The μSAXS pattern obtained before drawing clearly shows the four-leaf clover pattern originating from the cross-hatched structure, whereas only two disordered spots are observed in the μSAXS pattern after drawing. Highly anisotropic μWAXS patterns are also largely different before and after drawing. With respect to μSAXS changes during hot drawing, they calculated the sequences of long periods and full-widths at half-maximum (fwhm) of the scattering peak from the sector averaged SAXS profile originating from the parent

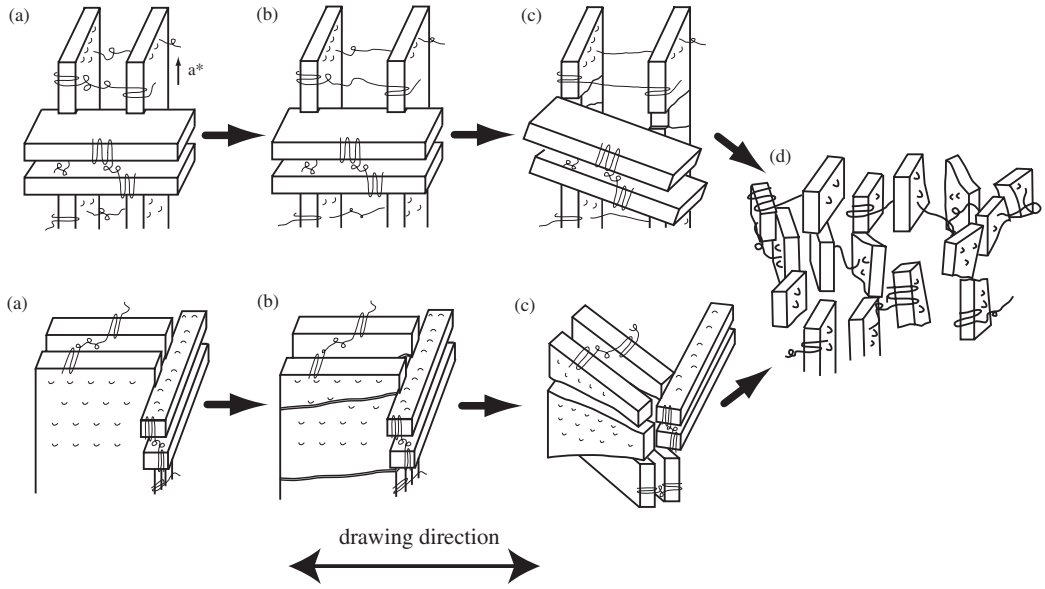


**Figure 15.** Deformation model of (upper) perpendicular and (lower) parallel lamellae in iPP: (a) initial state, (upper (b)) elongation of amorphous chain at first stage, (upper (c)) disordering of parent lamella crystal along *a*-axis and rotation of daughter lamellae at second stage, (lower (b)) disordering of crystal aloing *a*-axis, (lower (c)) rotation of parent lamellae followed by rotation of daughter lamellae, and (d) fragmentation at final stage (Reproduced with permission from ref 90. Copyright (2007) American Chemical Society).

and daughter lamellae, and obtained the information on the relationship between the change in long periods and the disordering of the stacking structure. With respect to μWAXS changes, they calculated the sequences of the fwhm and azimuthal distribution of each reflection and estimated the ordered crystal size and the degree of crystal orientation rearrangement. By these analyses, they identified the sequence of stress transfer inside the cross-hatched structure during hot drawing and constructed the detailed deformation model, as shown in Figure 15. Initially, the long period of the parent lamella simply increases, whereas no disordering of the stacking structure occurs, indicating that the stretching of the amorphous region between lamella crystals occurs before the disordering of the stacking structure. Next, the disordering of the lamella stacking structure and the decrease in the ordered crystal size of the parent lamella occur, whereas the crystal size of the daughter lamella does not decrease. Interestingly, the ordered crystal of the daughter lamella is initially smaller than that of the parent lamella and its size remains constant during drawing until a drastic rearrangement starts. Finally, a marked rearrangement of the crystal orientation occurs. They also performed the same experiment using polypropylene randomly copolymerized with butene (bPP) and observed a different deformation behavior from iPP.

The next application is related to the evaluation of stress transfer to the interface of matrix polymer and fiber in composites. In fiber-reinforced polymeric materials, the strength of interaction at the matrix polymer-fiber interface and the manner of stress transfer are examples of the most essential factors that control the mechanical strength.

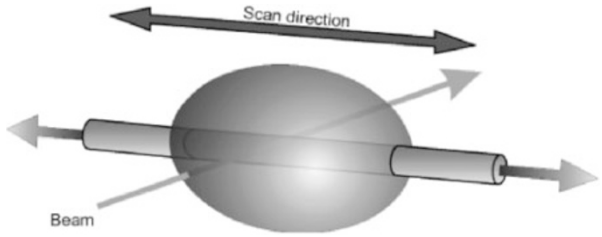


**Figure 16.** Schematic diagram of experimental setup for microdroplet specimen (Reprinted with permission from ref 91. Copyright (2004) American Chemical Society).

Young *et al.* performed a scanning microbeam WAXS experiment using epoxy resin matrix polymer/PBO single fiber composite with two different specimen geometries, namely an epoxy resin test piece including a single PBO fiber inside the piece and a single fiber covered with epoxy resin microdroplets[91] (see Figure 16). Here, we introduce an interesting result for a microdroplet geometry. They measured the crystal lattice constant of the fiber after drawing and determined the crystal strain $\varepsilon_c$ and stress $\sigma$ from the difference between the lattice constant in a deformed region ($c_s$) and that in a undeformed region ($c_0$) by the following formula using

$$\varepsilon_c = \frac{c_\sigma - c_0}{c_0}$$

$$E_c = \frac{\sigma}{\varepsilon_c},$$

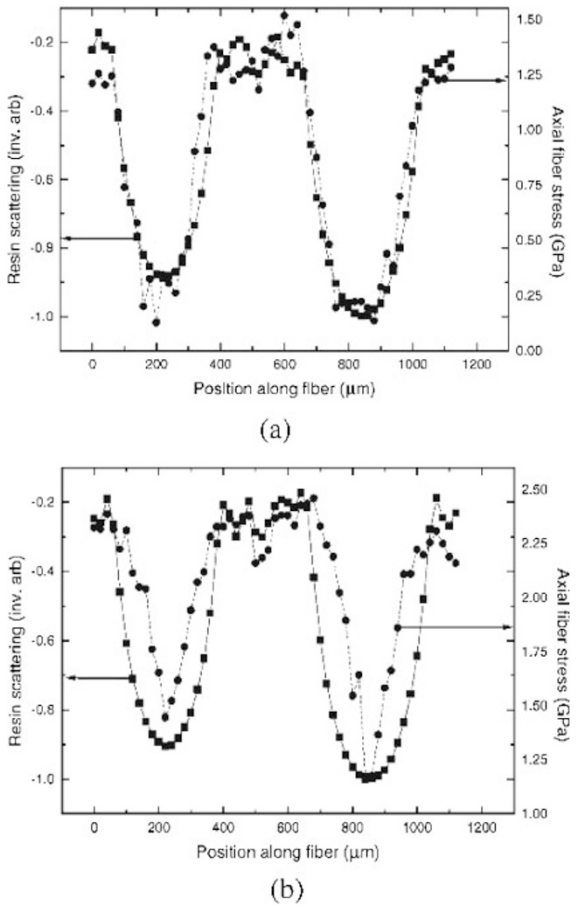


**Figure 17.** Superimposed plots of intensity of resin scattering multiplied by (−1) and axial fiber stress at same position along fiber for specimen at loads of (a) 15.1 g and (b) 27.7 g (Reprinted with permission from ref 91. Copyright (2004) American Chemical Society).

where $E_c$ is the crystal modulus. They scanned the drawn fiber sample in 20 μm steps along fiber with microbeam generated with K-B mirror optics (the beam size was 5 μm diameter), measured the lattice constant from a 004 reflection and obtained the spatial distribution of the stress applied to the PBO fiber. They found that the stress applied to the fiber decreases in the region where the epoxy resin microdroplets cover the fiber because the stress is equally distributed over the entire system, consisting of the epoxy and fiber. Then, they compared the degree of reduction in the stress applied to the fiber with the relative amount of epoxy resin that covers the fiber. The relative amount of epoxy resin matrix was obtained from the integrated scattering intensity of the amorphous epoxy resin. In Figure 17, the comparison between the amount of epoxy resin and the stress applied to the fiber at each position is shown. At a low stress, their patterns completely agree with each other, indicating that epoxy resin covering the fiber absorbs the stress in proportion to the volume of epoxy. However, at a high stress, they showed a clear discrepancy. This strongly indicates that the stress applied to the system cannot equally be absorbed in the system, destroying the interface between the epoxy resin and the PBO fiber and increasing the stress applied to the fiber.

*Indentation.* The next application is related to structural deformation by microindentation on a polymer fiber.[92,93] Indentation is a test method for pushing a sample using an indenter with a sharp head of a hard material, such as a square-based diamond pyramid, which is used to measure the hardness of materials. As for the stress transfer analyses inside materials, the spatial distribution of the deformed structure itself after indentation provides abundant information on the manner of stress transfer in materials, and *in situ* measurement during indentation provides supplementary information about elastic recovery to the final deformed structure formation. These pieces of information are essential for understanding the origin of the hardness of materials.

Gourrier *et al.* performed microbeam WAXS to observe the deformed structures of various polymer fibers during and after microindentation.[92] They developed the customized microindentation apparatus allowing one to adjust the position of a specimen precisely and to observe the specimen under an optical microscope. Here, we introduce the application of microindentation to Nylon66 and ultrahigh molecular weight polyethylene (UHMW-PE) fibers. First, they scanned samples after microindentation with a microbeam generated with the combination of focusing mirror and collimator (the beam size was 5 μm diameter) at 5 μm intervals. In Nylon66 after indentation, the degree of crystal orientation determined in the region immediately below the region of indenter tip penetration, which is analyzed from the azimuthal distribution of WAXS, is lower than that in the region without deformation, whereas crystallinity is the same between these regions. This indicates the local perturbation of crystal orientation by plastic deformation. In UHMW-PE, the deformation distribution is complex (see Figure 18). As for the degree of crystal orientation, the region 5 μm away from the indenter tip-polymer interface shows a low degree of crystal orientation, which is similar to that of Nylon66. Furthermore, the polymorph of PE which is an orthorhombic phase before indentation, was partially transformed to a monoclinic phase. In the region 10 μm away from the indenter tip-polymer interface, the monoclinic phase appeared. Interestingly, at a further region ($> 10$ μm), a split of orthorhombic crystal orientation was observed instead of a monoclinic phase. It is known that a force larger than the critical value is necessary for the phase transition to a monoclinic phase.[96] Therefore, this result indicates that an external force beyond the critical value was applied in the region

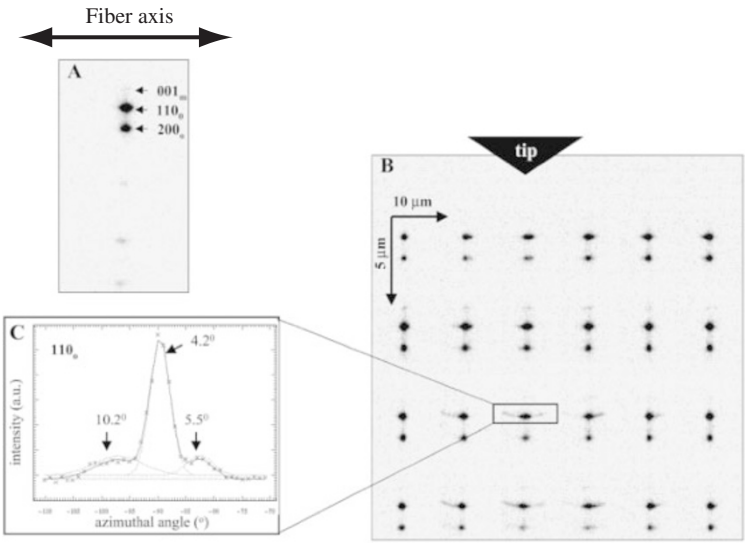


**Figure 18.** (A) Equatorial pattern of single UHMW-PE fiber. (B) Composite image of indented zone in UHMW-PE limited to $110_0/200_0$ and $001_m$ reflections. Mesh increments are $10 \times 5\,\mu m$. (C) Azimuthal profile of a selected frame, which can be fitted by three Gaussian functions corresponding to central domain and two satellite domains. The azimuthal width (fwhm) of the domains is indicated (Reprinted with permission from ref 92. Copyright (2002) American Chemical Society).

10 μm away from the indenter tip-polymer interface. It should also be noted that the crystal in the region nearest the tip-polymer interface shows no monoclinic phase but the slight broadening of the crystal orientation by plastic deformation, indicating that the stress is not well applied in this region. This might be due to the skin-core inner structure of the polymer fiber, though it is not discussed in the paper. Furthermore, they performed *in situ* microbeam WAXS during indentation. They fixed the position of a microbeam below the center of the fiber, located far from the indenter and observed a structural change during indentation. In this experiment, they clearly observed the splitting of a diffraction spot during indentation and its recovery to a single spot pattern when it was released, though its azimuthal distribution after indentation was broader than the original azimuthal distribution.

*Microphase Separated Morphology*

Among the applications of microbeam X-ray scattering, its application to an amorphous polymer system is very rare. However, interesting applications have recently been reported in the characterization of highly ordered microphase separated morphology in block polymers.[97–99]

Matsushita and coworkers have synthesized ABC star block copolymers with precisely controlled chain lengths by anionic polymerization and characterized their morphologies by TEM and microbeam SAXS.[97] They synthesized polyisoprene(I)-polysthyrene(S)-poly(2-vinyl pyridine)(P) star block copolymers. They systematically changed the length of the P chain and obtained an ISP star polymer with a chain volume ratio of I:S:P = 1:1:x (x = 0.7, 1.2, 1.9), which is coded as $I_{1.0}S_{1.0}P_x$. Furthermore, a polymer sample with x = 1.3 was also prepared by blending two samples, *i.e.*, $I_{1.0}S_{1.0}P_{1.2}$ and $I_{1.0}S_{1.0}P_{1.9}$, at a weight ratio of 0.85/0.15. These four samples showed typical Archimedean tiling patterns[100] and corresponding microbeam SAXS patterns were observed with microbeam generated with pinhole optics (the beam size was $5\,\mu m \times 5\,\mu m$), as shown in Figure 19. A clear correspondence between the results of TEM and microbeam SAXS guarantees that the structures observed by TEM are statistically most probable in the microbeam-irradiated area. This clearly shows that the most critical problem in TEM observation, *i.e.*, the lack of statistical accuracy, is completely resolved by microbeam SAXS experiment. It should also be noted that the good coincidence between the results of TEM and microbeam SAXS is realized because the beam size is comparable to the grain size.

They also performed other experiments by controlling the chain length and blending an ABC terpolymer with homopolymers, and found new tiling patterns that do not correspond to Archimedean tiling, which is statistically evidenced by microbeam SAXS.[98]

## PERSPECTIVES

As is described in the above, a microbeam X-ray scattering technique can be widely applied to the characterization of polymeric materials having spatial inhomogeneity. In the near future, more experimental results are expected to be obtained by microbeam X-ray scattering. We suggest the following advanced

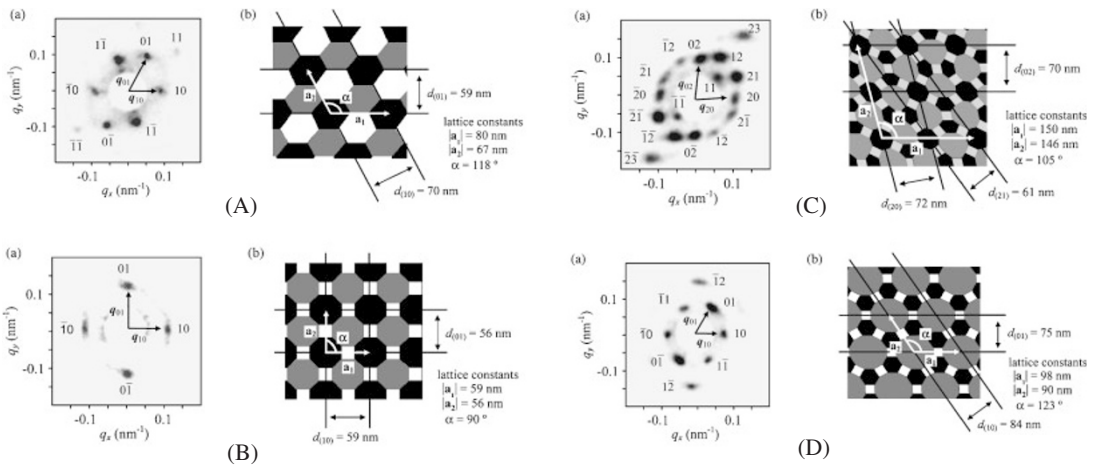


**Figure 19.** Microbeam SAXS patterns (a) and corresponding schematic tiling structures (b) of (A) $I_{1.0}S_{1.0}P_{0.7}$, (B) $I_{1.0}S_{1.0}P_{1.2}$, (C) $I_{1.0}S_{1.0}P_{1.3}$, and (D) $I_{1.0}S_{1.0}P_{1.9}$ (Reproduced with permission from ref 97. Copyright (2006) American Chemical Society).

experiments related to the application of microbeam X-ray scattering introduced in this review: 1) the time-resolved μSAXS-WAXS measurement of a local crystallization behavior at various positions in banding spherulite having a discontinuous twisting structure, which enables us to elucidate the relationship between rhythmic growth and discontinuous twisting, 2) time-resolved μSAXS-WAXS measurement for verifying melt recrystallization during drawing, which has been controversial until now,[101,102] and 3) time-resolved and scanning μSAXS-WAXS measurements for investigating stress transfer in fibrous materials with a skin-core morphology during uniaxial drawing, which is directly related to the mechanical strength in fibers.

In addition to the microbeam X-ray scattering techniques shown in this review, it is worth mentioning that microbeam grazing-incidence SAXS (GI-SAXS) is a powerful tool for analyzing surface structures having spatial inhomogeneity,[103,104] and that X-ray photon correlation spectroscopy (XPCS) is a unique method for analyzing the slow dynamics of nanostructures such as block copolymers and filled rubbers.[105,106]

Finally, we would refer to the present situation of synchrotron radiation beamlines for microbeam X-ray scattering in Japan. There exist beamlines used for microbeam SAXS/WAXS experiments. However, there is no beamline dedicated for microbeam SAXS-WAXS in SPring-8, whereas other third-generation synchrotron sources, such as ESRF, APS and BESSY II, have beamlines dedicated for microbeam SAXS-WAXS. This situation limits microbeam SAXS/WAXS research activities in polymer science in Japan considerably when compared with those in other countries. This should be improved urgently in order to advance and widen synchrotron radiation research in polymer science and technology.

## REFERENCES


1. F. J. Baltá Callejá, D. C. Bassett, and A. Keller, *Polymer*, **4**, 269 (1963).
2. T. Albrecht and G. Strobl, *Macromolecules*, **28**, 5827 (1995).
3. S. Nojima, K. Kato, S. Yamamoto, and T. Ashida, *Macromolecules*, **25**, 2237 (1992).
4. G. Shin, N. Sakamoto, K. Saijo, S. Suehiro, T. Hashimoto, K. Ito, and Y. Amemiya, *Macromolecules*, **33**, 9002 (2000).
5. R. S. Justice, D. W. Schaefer, R. A. Vaia, D. W. Tomlin, and T. J. Bunning, *Polymer*, **46**, 4465 (2005).
6. T. P. Rieker, M. Hindermann-Bischoff, and F. Ehrburger-Dolle, *Langmuir*, **16**, 5588 (2000).
7. Y. Amemiya, K. Ito, N. Yagi, Y. Asano, K. Wakabayashi, T. Ueki, and T. Endo, *Rev. Sci. Instrum.*, **66**, 2290 (1995).
8. M. W. Tate, D. Chamberlain, and S. M. Gruner, *Rev. Sci. Instrum.*, **76**, 081301 (2005).
9. S. M. Gruner, M. W. Tate, and E. F. Eikenberry, *Rev. Sci. Instrum.*, **73**, 2842 (2002).
10. Y. Amemiya and J. Miyahara, *Nature*, **336**, 89 (1988).
11. Y. Amemiya, *J. Synchrotron Rad.*, **2**, 13 (1995).
12. N. Yagi and K. Inoue, *J. Appl. Crystallogr.*, **40**, s439 (2007).
13. R. Lewis, W. Helsby, A. Jones, C. Hall, B. Parker, J. Sheldon, P. Clifford, M. Hillen, I. Summer, N. Fore, R. Jones, and K. Roberts, *Nucl. Instrum. Methods*, **A392**, 32 (1997).
14. B. S. Hsiao, B. B. Sauer, R. K. Verma, H. G. Zachmann, S. Seifert, B. Chu, and P. Harney, *Macromolecules*, **28**, 6931 (1995).
15. E. L. Heeley, A. V. Maidens, P. D. Olmsted, W. Bras, I. P. Dolbnya, J. P. A. Fairclough, N. J. Terrill, and A. J. Ryan, *Macromolecules*, **36**, 3656 (2003).
16. G. Kumaraswamy, J. A. Kornfield, F. Yeh, and B. S. Hsiao, *Macromolecules*, **35**, 1762 (2002).
17. M. Imai, K. Kaji, and T. Kanaya, *Macromolecules*, **27**, 7103 (1994).

18. T. Sakurai, Y. Nozue, T. Kasahara, K. Mizunuma, N. Yamaguchi, K. Tashiro, and Y. Amemiya, *Polymer*, **46**, 8846 (2005).
19. S. Toki and B. S. Hsiao, *Macromolecules*, **36**, 5915 (2003).
20. S. Ran, X. Zong, D. Fang, B. S. Hsiao, B. Chu, and R. A. Phillips, *Macromolecules*, **34**, 2569 (2001).
21. M. F. Butler, A. M. Donald, and A. J. Ryan, *Polymer*, **38**, 5521 (1997).
22. A. Mahendrasingam, D. J. Blundell, M. Parton, A. K. Wright, J. Rasburn, T. Narayanan, and W. Fuller, *Polymer*, **46**, 6009 (2005).
23. A. A. Apostolov, S. Fakirov, M. Stamm, R. D. Patil, and J. E. Mark, *Macromolecules*, **33**, 6856 (2000).
24. J. J. Ge, A. Zhang, K. W. McCreight, S. Y. Wang, F. W. Harris, and S. Z. D. Cheng, *Macromolecules*, **31**, 4093 (1998).
25. K. Tashiro and R. Tanaka, *Polymer*, **47**, 5433 (2006).
26. J. A. Pople, I. W. Hamley, J. P. A. Fairclough, A. J. Ryan, B. U. Komanschek, A. J. Gleeson, G. E. Yu, and C. Booth, *Macromolecules*, **30**, 5721 (1997).
27. A. Keller, *J. Polym. Sci.*, **17**, 291 (1955).
28. http://www.esrf.eu/UsersAndScience/Experiments/SCMatter/ID13/
29. M. Müller, M. Burghammer, and C. Riekel, *Nucl. Instrum. Methods*, **A467**, 958 (2001).
30. https://beam.aps.anl.gov/pls/apsweb/beamline_display_pkg.display_beamline?p_beamline_num_c=17
31. http://www.spring8.or.jp/wkg/BL40XU/instrument/lang-en/INS-0000000353/instrument_summary_view
32. http://www.bessy.de/users_info/02.beamlines/linespdf/ID_02_1.pdf
33. O. Paris, C. Li, S. Siegel, G. Weseloh, F. Emmerling, H. Riesemeier, A. Erko, and P. Fratzl, *J. Appl. Crystallogr.*, **40**, s466 (2007).
34. http://pfwww.kek.jp/users_info/users_guide_e/station_spec_e/bl04/bl4a.html
35. A. Iida and T. Noma, *Nucl. Instrum. Methods*, **B82**, 129 (1993).
36. C. Riekel, *Rep. Prog. Phys.*, **63**, 233 (2000).
37. P. Kirkpatrick and A. V. Baez, *J. Opt. Soc. Am.*, **38**, 766 (1948).
38. A. Snigirev, V. Kohn, I. Snigireva, and B. Lengeler, *Nature*, **384**, 49 (1996).
39. Y. Suzuki, A. Takeuchi, H. Takano, T. Ohigashi, and H. Takenaka, *Jpn. J. Appl. Phys.*, **40**, 1508 (2001).
40. S. Kuznetsov, I. Snigireva, A. Snigirev, P. Engström, and C. Riekel, *Appl. Phys. Lett.*, **65**, 827 (1994).
41. M. Müller, M. Burghammer, D. Flot, C. Riekel, C. Morawe, B. Murphy, and A. Cedora, *J. Appl. Crystallogr.*, **33**, 1231 (2000).
42. K. Inoue, T. Oka, T. Suzuki, N. Yagi, K. Takeshita, S. Goto, and T. Ishikawa, *Nucl. Instrum. Methods*, **A467**, 674 (2001).
43. J. J. Point, *Bull. Acad. R. Belg.*, **41**, 982 (1955).
44. H. D. Keith and F. J. Padden, *Polymer*, **25**, 28 (1984).
45. J. C. Lee, H. Tazawa, T. Ikehara, and T. Nishi, *Polym. J.*, **30**, 327 (1998).
46. J. C. Lee, H. Tazawa, T. Ikehara, and T. Nishi, *Polym. J.*, **30**, 780 (1998).
47. F. J. Padden and H. D. Keith, *J. Appl. Phys.*, **37**, 4013 (1966).
48. R. Verma, H. Marand, and B. Hsiao, *Macromolecules*, **29**, 7767 (1996).
49. B. S. Hsiao, Z. Wang, F. Yeh, Y. Gao, and K. C. Sheth, *Polymer*, **40**, 3515 (1999).
50. R. Kolb, C. Wutz, N. Stribeck, G. von Krosigk, and C. Riekel, *Polymer*, **42**, 5257 (2001).
51. Y. Nozue, R. Kurita, S. Hirano, N. Kawasaki, S. Ueno, A. Iida, T. Nishi, and Y. Amemiya, *Polymer*, **44**, 6397 (2003).
52. Y. Nozue, S. Hirano, N. Kawasaki, S. Ueno, N. Yagi, T. Nishi, and Y. Amemiya, *Polymer*, **45**, 8593 (2004).
53. M. Seki, D. W. Thurman, J. P. Oberhauser, and J. A. Kornfield, *Macromolecules*, **35**, 2583 (2002).
54. J. K. Keum, R. H. Somani, F. Zuo, C. Burger, I. Sics, B. S. Hsiao, H. Chen, R. Kolb, and C. T. Lue, *Macromolecules*, **38**, 5128 (2005).
55. S. Ran, C. Burger, D. Fang, X. Zong, B. Chu, B. S. Hsiao, Y. Ohta, K. Yabuki, and P. M. Cunniff, *Macromolecules*, **35**, 9851 (2002).
56. S. Mitsuhashi, *Bull. Text. Res. Inst.*, **66**, 1 (1963).
57. S. Kimata, T. Sakurai, Y. Nozue, T. Kasahara, N. Yamaguchi, T. Karino, M. Shibayama, and J. A. Kornfield, *Science*, **316**, 1014 (2007).
58. C. Riekel, B. Madsen, D. Knight, and F. Vollrath, *Biomacromolecules*, **1**, 622 (2000).
59. M. C. Garcia Gutierrez, G. C. Alfonso, C. Riekel, and F. Azzurri, *Macromolecules*, **37**, 478 (2004).
60. H. D. Keith, F. J. Padden, and T. P. Russel, *Macromolecules*, **22**, 666 (1989).
61. C. Riekel, M. Mueller, and F. Vollrath, *Macromolcules*, **32**, 4464 (1999).
62. C. Riekel and F. Vollrath, *Int. J. Biol. Macromol.*, **29**, 203 (2001).
63. H. D. Keith and F. J. Padden, *Macromolecules*, **29**, 7776 (1996).
64. I. Saracovan, H. D. Keith, R. J. Manley, and G. R. Brown, *Macromolecules*, **32**, 8918 (1999).
65. K. L. Singfield, J. M. Klass, and G. R. Brown, *Macromolecules*, **28**, 8006 (1995).
66. Y. Nozue, S. Hirano, R. Kurita, N. Kawasaki, S. Ueno, A. Iida, T. Nishi, and Y. Amemiya, *Polymer*, **45**, 8299 (2004).
67. T. Kyu, H. W. Chiu, A. J. Gruenthner, Y. Okabe, H. Saito, and T. Inoue, *Phys. Rev. Lett.*, **83**, 2749 (1999).
68. M. Gazzano, M. L. Focarete, C. Riekel, and M. Scandola, *Biomacromolecules*, **5**, 553 (2004).
69. J. Karger-Kocsis, *Polym. Eng. Sci.*, **36**, 203 (1996).
70. A. J. Lovinger, J. O. Chua, and C. C. Gryte, *J. Polym. Sci. Polym. Phys. Ed.*, **15**, 641 (1977).
71. A. Lustiger, C. N. Marzinsky, R. R. Mueller, and H. D. J. Wagner, *Adhs.*, **53**, 1 (1995).
72. P. Zipper, A. Janosi, E. Wrentschur, P. M. Abuja, and C. Knabl, *Prog. Colloid Polym. Sci.*, **93**, 377 (1993).
73. J. Torre, M. Cortázar, M. A. Gómez, C. Marco, G. Ellis, C. Riekel, and P. Dumas, *Macromolecules*, **39**, 5564 (2006).
74. C. Riekel, T. Dieing, P. Engstrom, L. Vincze, C. Martin, and A. Mahendrasingam, *Macromolecules*, **32**, 7859 (1999).
75. A. C. Hermes, R. J. Davies, S. Greiff, H. Kutzke, S. Lahlil,

P. Wyeth, and C. Riekel, *Biomacromolecules*, **7**, 777 (2006).
76. C. Riekel, A. Cedola, F. Heidelbach, and K. Wagner, *Macromolecules*, **30**, 1033 (1997).
77. T. Tanaka, M. Fujita, A. Takeuchi, Y. Suzuki, K. Uesugi, K. Ito, T. Fujisawa, Y. Doi, and T. Iwata, *Macromolecules*, **39**, 2940 (2006).
78. T. Iwata, Y. Aoyagi, T. Tanaka, M. Fujita, A. Takeuchi, Y. Suzuki, and K. Uesugi, *Macromolecules*, **39**, 5789 (2006).
79. J. Schoeck, R. J. Davies, A. Martel, and C. Riekel, *Biomacromolecules*, **8**, 602 (2007).
80. M. Muller, C. Czihak, G. Vogl, P. Fratzl, H. Schober, and C. Riekel, *Macromolecules*, **31**, 3953 (1998).
81. M. Müller, C. Riekel, R. Vuong, and H. Chanzy, *Polymer*, **41**, 2627 (2000).
82. L. Kreplak, C. Mérigoux, F. Briki, D. Flot, and J. Doucet, *Biochim. Biophys. Acta.*, **1547**, 268 (2001).
83. D. Lozano-Castelló, E. Raymundo-Piñero, D. Cazorla-Amorós, A. Linares-Solano, M. Müller, and C. Riekel, *Carbon*, **40**, 2727 (2002).
84. R. J. Davies, M. Burghammer, and C. Riekel, *Macromolecules*, **38**, 3364 (2005).
85. S. Roth, M. Burghammer, A. Janotta, and C. Riekel, *Macromolecules*, **36**, 1585 (2003).
86. Y. Kajiura, S. Watanabe, T. Itou, K. Nakamura, A. Iida, K. Inoue, N. Yagi, Y. Shinohara, and Y. Amemiya, *J. Struct. Biol.*, **155**, 438 (2006).
87. C. Riekel, *Nucl. Instrum. Methods*, **B199**, 106 (2003).
88. "The Science of Hair Care," 2nd ed, C. Bouillon and J. Wilkinson, Ed., CRC Press, 2005.
89. M. Horio and T. Kondo, *Text. Res. J.*, **23**, 388 (1953).
90. Y. Nozue, Y. Shinohara, Y. Ogawa, T. Sakurai, H. Hori, T. Kasahara, N. Yamaguchi, N. Yagi, and Y. Amemiya, *Macromolecules*, **40**, 2036 (2007).
91. R. J. Young, S. J. Eichhorn, Y. T. Shyng, C. Riekel, and R. J. Davies, *Macromolecules*, **37**, 9503 (2004).
92. A. Gourrier, M. C. García Gutiérrez, and C. Riekel, *Macromolecules*, **35**, 8072 (2002).
93. A. Gourrier, M. C. García Gutiérrez, and C. Riekel, *Macromolecules*, **38**, 3838 (2005).
94. R. J. Davies, M. Burghammer, and C. Riekel, *Macromolecules*, **39**, 4834 (2006).
95. C. Lorenz-Haas, P. Müller-Buschbaum, O. Wunnicke, C. Cassignol, M. Burghammer, C. Riekel, and M. Stamm, *Langmuir*, **19**, 3056 (2003).
96. T. Seto, T. Hara, and K. Tanaka, *Jpn. J. Appl. Phys.*, **7**, 31 (1968).
97. K. Hayashida, W. Kawashima, A. Takano, Y. Shinohara, Y. Amemiya, Y. Nozue, and Y. Matsushita, *Macromolecules*, **39**, 4869 (2006).
98. K. Hayashida, A. Takano, S. Arai, Y. Shinohara, Y. Amemiya, and Y. Matsushita, *Macromolecules*, **39**, 9402 (2006).
99. Y. Matsushita, *Macomolecules*, **40**, 771 (2007).
100. B. Grunbaum and G. C. Shephard, in "Tilings and Patterns," Freeman, New York, 1986.
101. P. J. Flory and D. Y. Yoon, *Nature (London)*, **272**, 226 (1978).
102. D. M. Sadler and P. J. Barham, *Polymer*, **31**, 36 (1990).
103. C. Nicolini and E. Pechkova, *J. Cell. Biochem.*, **97**, 544 (2006).
104. E. Pechkova, S. V. Roth, M. Burghammer, D. Fontani, C. Riekel, and C. Nicolini, *J. Synchrotron Radiat.*, **12**, 713 (2005).
105. M. L. Ruegg, A. J. Patel, S. Narayanan, A. R. Sandy, S. G. J. Mochrie, H. Watanabe, and N. P. Balsara, *Macromolecules*, **39**, 8822 (2006).
106. Y. Shinohara, H. Kishimoto, T. Maejima, H. Nishikawa, N. Yagi, and Y. Amemiya, *Jpn. J. Appl. Phys.*, **46**, L300 (2007).

Yoshinobu Nozue was born in Kanagawa Prefecture, Japan in 1974. He received his B.S degree in 1997, M.S. degree in 1999 and Ph.D. degree in 2002 from The University of Tokyo under the supervision of Professor Yoshiyuki Amemiya. He investigated the fading property of imaging plate, which is a two-dimensional X-ray detector widely used, and suggested the fading mechanism in B.S. From master's course, he has had strong interests in the complexity of soft materials and the beauty of structure analysis in small-angle scattering. Since then, he has concentrated on the structure analyses of soft materials, such as peptide-lipid complex and crystalline polymer blends, using small-angle X-ray scattering. In particular, he started the application of microbeam X-ray scattering to polymeric materials in his doctoral program. After his graduation, he moved to Sumitomo Chemical Co. Ltd. On the occasion of his movement to Sumitomo, he started the characterization of polymer systems using small-angle neutron scattering. Present research interests of Dr. Nozue are as follows: (1) Advanced applications of X-ray and neutron scattering to polymers; (2) Research and development of polymeric materials, especially polyolefins, through structure controls. He was the recipient of several awards, *e.g.*, The scientific award of Japanese Society for Synchrotron Radiation Research (JSSRR) (2006) and The Awards of Crystallographic Society of Japan (CrSJ), Young Crystallographer Award (2007).

Yuya Shinohara was born in Tokyo Prefecture, Japan in 1981. He received his B.S. degree in 2003 and M.S. degree in 2005 from The University of Tokyo under the supervision of Professor Yoshiyuki Amemiya. He left university without getting a Ph.D. and was promoted to assistant professor in 2007 at the same institution. His present research interests are divided into three areas: (1) Structural analysis of soft materials using small-angle X-ray scattering; (2) Dynamics of soft materials using X-ray photon correlation spectroscopy; (3) Development of novel measurements using X-rays.

Yoshiyuki Amemiya was born in Tokyo Prefecture, Japan in 1952. He received his B.S. degree in 1974, M.S. degree in 1976, and Ph.D. degree in 1979 from The University of Tokyo under the supervision of Professor Kazutake Kohra. He moved to Photon Factory, National Laboratory for High Energy Physics (KEK) as a JSPS research fellow in 1979, where he had been a beamline manager of BL-15A (Small-Angle X-ray Scattering) until 1996. He was promoted to research assistant in 1982 and to associate professor in 1989 at the same institution. In 1988, he started to study the X-ray ellipsometry in Brookhaven National Laboratory as a visiting fellow. He moved to The University of Tokyo in 1996 and was promoted to full professor in 1998 at the same institution. From 2007, he has been the dean of Graduate School of Frontier Sciences, The University of Tokyo. Present research interests of Professor Amemiya are (1) development and application of time-resolved small-angle X-ray scattering, (2) development of high-performance X-ray detector, (3) development and application of X-ray ellipsometry. He is the recipient of several awards, *e.g.*, The Award of the Crystallographic Society of Japan (2001).